JCTC Journal of Chemical Theory and Computation

Ionization-Induced Structural Changes in Uracil Dimers and Their Spectroscopic Signatures

Anna A. Zadorozhnaya and Anna I. Krylov*

Department of Chemistry, University of Southern California, Los Angeles, California 90089-0482

Received September 29, 2009

Abstract: The electronic structure of the three representative isomers of the ionized uracil dimers is characterized by high-level electronic structure calculations. Noncovalent interactions between the fragments lower the vertical ionization energies by 0.13−0.35 eV, the largest drop being observed for the stacked and the T-shaped isomers. The initial hole is delocalized in the stacked and the H-bonded isomers and is localized in the T-shaped one. The ionization induces significant structural relaxation and increases the binding energies. The stacked dimer cation relaxes to the symmetric structure bound by 22.7 kcal/mol. The T-shaped dimer cation has a binding energy of 25.1 kcal/mol. Thus, the relative order of the stacked and T-shaped isomers is reversed upon ionization. Finally, the H-bonded isomer, which relaxes to the proton-transferred structure, is bound by 37.0 kcal/mol. The electronic spectra of all three isomers characterized at the vertical and the relaxed geometries show different patterns, which may be exploited in spectroscopic probing of ionization-induced dynamics in these species.

1. Introduction

The ionization-induced changes in DNA, which are responsible for oxidative and radiative damage of the genetic material, involve complicated coupled electron−nuclear dynamics.[1–6] The hole migration is facilitated by thermal fluctuations, which affect the ionization energies (IEs) of the individual bases, and is coupled to proton transfer. Understanding how the local environment modulates the electronic properties of nucleobases is the first step toward developing a mechanistic picture of these processes.

Gas-phase studies of small nucleobase clusters reveal the intrinsic properties of these species and allow one to quantify different effects present in realistic environments.[7] Nucleobase dimers are convenient model systems on which the effects of different types of noncovalent interactions (i.e., π-stacking, H-bonding, and electrostatics) on the electronic structure and ionization-induced dynamics can be studied by combination of state-of-the art experimental techniques and high-level theoretical methods. While the IEs of the nucleic acid bases in the gas phase have been characterized both experimentally[8–14] and computationally,[15–18] much less is known quantitatively about the effects of different interactions on the IEs in realistic environments.

Our recent combined theoretical and experimental study[19] of the homo- and heterodimers of adenine and thymine demonstrated that noncovalent interactions lower the vertical IEs by as much as 0.4 eV and that the effect is larger for thymine than for adenine. Thus, these interactions reduce the differences between the IEs of the purines and pyrimidines and promote hole migration. The magnitude and origin of the effect are different for different isomers. The largest drop in IEs was observed in the symmetric stacked and nonsymmetric H-bonded dimers. In the former case, the IE is lowered due to the hole delocalization over the two fragments and the change depends on the overlap between the fragments' molecular orbitals (MOs). In the latter case, the overlap does not play an important role: the hole, which is localized on one of the fragments, is stabilized by the electrostatic interactions with the "neutral" fragment. The magnitude of the IE drop is determined by the magnitude and relative orientation of the dipole moment of the spectator fragment. The changes of the IEs due to H-bonding in the symmetric

* Corresponding author phone: (213) 740-4929; e-mail: krylov@usc.edu.

10.1021/ct900515a
Published on Web 01/27/2010

H-bonded dimers were found to be smaller.[19] A similar trend was observed for H-bonded cytosine dimers.[20]

Similar effects of π-stacking and H-bonding on the vertical IEs of the uracil dimer have been characterized in our previous work using high-level electronic structure calculations.[21] Earlier studies of the effects of π-stacking on the IEs of nucleobases include Hartree−Fock and DFT estimates using the Koopmans theorem[22–26] and MP2 (Møller−Plesset perturbation theory) and CASPT2 (perturbatively corrected complete active space self-consistent field) calculations.[15,17,27]

In agreement with simple MO considerations, ionization changes the bonding in the dimers, resulting in significant structural relaxation. Ionization increases the binding energy, yields tighter structures, and changes the relative stability of different isomers. Moreover, in H-bonded dimers it may initiate barrierless (or almost barrierless) proton transfer, which is believed to be coupled to hole hopping.[4–6,19,22,28–30] While the ionization-induced dynamics may be very complex and its modeling requires full-dimensional coupled nuclear and electronic dynamics calculations (e.g., as in the recent study of uracil),[18] the key features of these processes can be learned from analyzing differences in the electronic states and structural parameters at the initial and the relaxed geometries (i.e., equilibrium structures of the neutral and the cation, respectively). The focus of this work is on the ionization-induced changes in the structures, binding energies, and electronic states of representative isomers of the uracil dimer. We also discuss spectroscopic signatures of the relaxation, which may be exploited in time-resolved experiments.

An interesting feature of the noncovalent dimers is the appearance of strong so-called charge-resonance (CR) bands[31] in their electronic spectra upon ionization.[32–34] These bands correspond to the transitions between the dimer molecular orbitals (DMOs) that are in-phase and out-of-phase combinations of the fragment molecular orbitals (FMOs) and are unique to the ionized dimers. Thus, they can be used as a spectroscopic probe of the ionized dimer formation. Moreover, their energies and intensities depend strongly on the overlap of FMOs and are, therefore, very sensitive to the relative orientation of and the distance between the fragments. Thus, these bands can be exploited for obtaining structural information, including ionization-induced dynamics. Other electronic transitions, which correlate with the transitions in the monomers and are called local excitations (LEs), can provide additional information. Recently, we characterized the electronic spectra in several benzene dimer isomers,[35,36] water dimers,[37,38] and two isomers of the uracil dimer.[21] While the CR bands are most intense in the symmetric dimers with favorable orbital overlap (e.g., the sandwich benzene dimer or stacked uracil dimer), they also appear in the isomers with nonequivalent fragments and more localized states (e.g., some water dimers or the T-shaped benzene dimer) where they acquire partial charge-transfer character.

Nucleobase dimers form numerous isomers.[39–42] We consider three representative isomers of the uracil dimer: H-bonded, π-stacked, and T-shaped isomers. On the neutral potential energy surface (PES), the H-bonded isomer is the lowest in energy, followed by the π-stacked and the T-shaped isomers. As demonstrated below, ionization changes the binding energies and relative ordering of the isomers. On the cation PES, the lowest energy structure corresponds to the proton-transferred H-bonded dimer, followed by the T-shaped and stacked dimers. The symmetric H-bonded cation does not have a stable minimum and undergoes barrierless proton transfer. We analyze the differences between the isomers as well as their spectroscopic signatures by using qualitative molecular orbital and electrostatic considerations, i.e., within the dimer molecular orbital−linear combination of fragment molecular orbitals (DMO−LCFMO) model.[35,37]

The structure of the paper is as follows. In section 2, we discuss the theoretical methods and computational details. In section 3 we discuss the electronic structure of the ionized dimers (section 3.1) and their equilibrium geometries (section 3.2), energetics (section 3.3), and electronic spectroscopy (section 3.4). Our concluding remarks are given in section 4. The benchmark results for density functional theory (DFT) with long-range corrected functionals augmented by empirical dispersion terms are presented in the Appendix.

2. Theoretical Methods and Computational Details

Electronic structure calculations of dimer cations are challenging owing to the open-shell character of these species. The wave function methods that are based on open-shell doublet references are often plagued by symmetry breaking and spin contamination of the underlying open-shell Hartree−Fock (HF) reference.[43,44] DFT calculations suffer from self-interaction error,[45,46] which results in artificial charge delocalization.

Within the wave function formalism, these systems are best described by the equation-of-motion coupled-cluster method for ionization potentials, EOM-IP-CCSD or simply IP-CCSD,[36,47–50] and by its less expensive configuration interaction approximation, IP-CISD.[51] EOM-IP-CCSD and IP-CISD describe problematic doublet wave functions as ionized states derived from a well-behaved closed-shell wave function; i.e., the target open-shell wave functions are generated by a Koopmans-like excitation operator R acting on the reference wave function:

$$\Psi^{\text{EOM-IP}}(N-1) = \hat{R}\Psi_0(N) \tag{1}$$

where $\Psi_0(N)$ is the wave function of the N-electron neutral system and R consists of 1h and 2h1p (one hole and two hole one particle, respectively) operators generating $(N-1)$-electron determinants from the N-electron reference. In the more accurate IP-CCSD method, Ψ_0 is a correlated CCSD wave function, whereas Ψ_0 in IP-CISD is just a single Slater determinant. The amplitudes of R are found by diagonalization of the similarity-transformed (IP-CCSD) or bare (IP-CISD) Hamiltonian.

In the DFT methods, self-interaction error can be mitigated by including long-range Hartree−Fock exchange.[52–54] We employed the ωB97X-D functional,[55] which also includes empirical dispersion terms.[56] The empirical dispersion terms

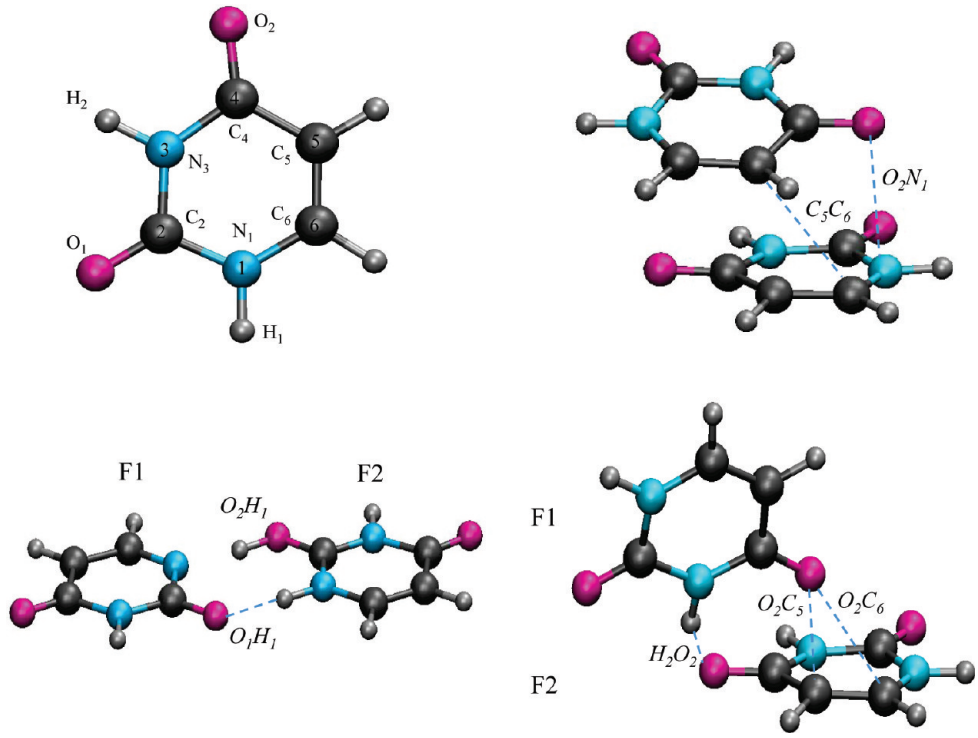

Figure 1. Definitions of the intra- and interfragment geometric parameters for uracil dimer isomers.

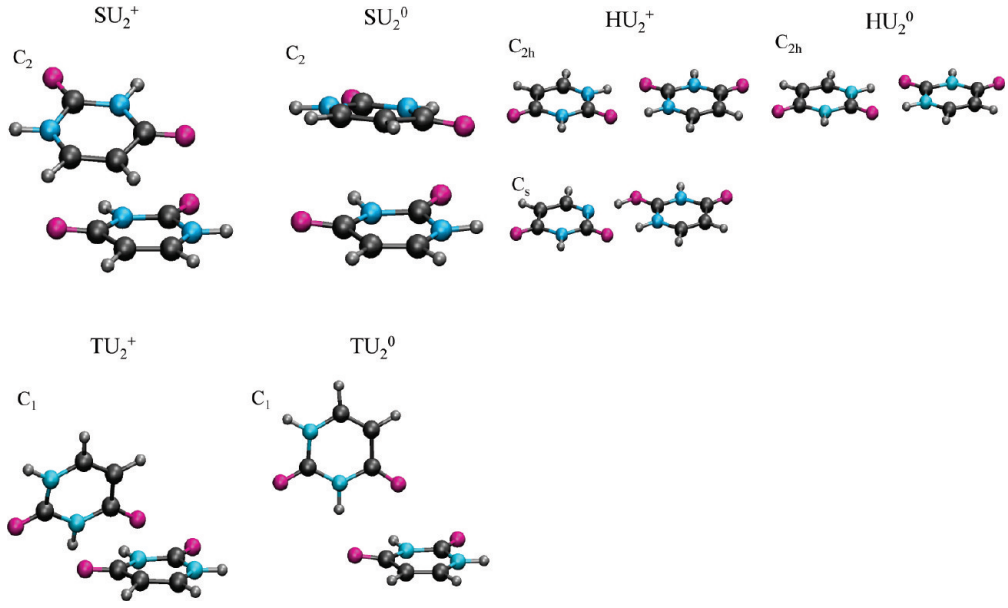

Figure 2. Geometries of the cations versus the respective neutrals for the three uracil dimer isomers.

partially mitigate the effects of basis set superposition error (BSSE) when used with an adequate basis set.

Throughout this work, we use the following notations for the isomers: HU_2, SU_2, and TU_2 refer to the H-bonded, stacked, and T-shaped isomers, respectively. For the hydrogen-bonded cations, we distinguish between the symmetric structure, which is a transition state (TS), and a proton-transferred one (PT) corresponding to the true minimum. The definitions of the inter- and intrafragment structural parameters for the stacked, T-shaped, and H-bonded isomers are given in Figure 1. The values of these parameters in the neutral and ionized systems are summarized in Tables 7 and 8. The changes in the structures induced by ionization are visualized in Figure 2.

We used EOM-IP-CCSD in calculations of the IEs, electronic spectra, and dissociation energies of the dimers, whereas for geometry optimizations and frequencies we employed IP-CISD and ωB97X-D. IP-CISD with the 6-31(+)G* basis[57] was used to optimize the SU_2^+ and HU_2^+ (TS) structures. The TU_2^+ and HU_2^+ (PT) structures were optimized with ωB97X-D and the 6-311(+)G** basis set.[58]

For both the IP-CISD and DFT-D optimizations, tight convergence criteria were enforced: the gradient and energy tolerance were set to 3×10^{-5} and 1.2×10^{-4}, respectively,

and the maximum energy change was set to 1×10^{-7}. To ensure the accuracy of the DFT-D optimizations, we employed the extrafine EML(99,590) grid.

We use the best available geometries for calculations of energy differences. The choice of the geometries is described below. In calculations of vertical properties (i.e., at the equilibrium geometries of the neutral dimers) we used the geometries from the S22 set of Hobza and co-workers.[59] The geometry of the T-shaped isomer was optimized with DFT-D as described above. To assess the possible effect of the BSSE on the structures, our study of adenine and thymine dimers[19] compared the B3LYP-D/6-31+G(d,p)-optimized structure of the stacked AT dimer versus that from the S22 set.[59] We found that the interfragment distance differs from the BSSE-corrected RI-MP2/TZVPP value[59] by only 0.076 Å. The increase of the basis set from 6-31G(d,p) to 6-311++G(2df,2pd) results in a 0.004 Å increase in interfragment separation. Thus, we do not expect significant BSSE effects on our optimized structures.

In the monomer calculations, we used the structures of the uracil cation and the neutral optimized by IP-CISD/6-31(+)G* and RI-MP2/cc-pVTZ, respectively, with the standard convergence thresholds (the gradient and energy tolerance were 3×10^{-4} and 1.2×10^{-3}, and maximum energy change was 1×10^{-6}). In all optimizations of the symmetric structures [i.e., all isomers, except for TU_2^0, TU_2^+, and HU_2^+ (PT)] the symmetry was enforced. For the stacked dimer cation we carried out an additional DFT-D optimization without the C_2 symmetry constraint that showed that the minimum indeed corresponds to the symmetric structure. In addition, vibrational analysis was performed.

For accurate energy estimates, single-point calculations were carried out at the geometries obtained as described above. The IP-CCSD method with the 6-311(+)G** basis was employed. For benchmark purposes, we also present ωB97X-D/6-311(+)G**/EML(99,590) estimates calculated at the respective DFT-D minima. The performance of different methods is discussed in the Appendix.

While the BSSE corrections can be substantial for weakly bound systems when compact basis sets are employed,[27,59,60] using augmented triple-ζ bases reduces the BSSE considerably. Moreover, empirical dispersion correction in DFT-D methods mitigates the BSSE. For example, the counterpoise correction for the binding energy in the stacked adenine−thymine dimer at the B3LYP-D/6-311+G(2df) level is only 1.4 kcal/mol.[19,61]

For the neutral stacked uracil dimer, the ωB97X-D and CCSD values of D_e are 10.5 and 11.1 kcal/mol (with the 6-311(+)G(d,p) basis set), in good agreement with the CCSD(T)/CBS value of 9.7 kcal/mol.[62] Thus, the BSSE effects are relatively small at the ωB97X-D/6-311(+)G(d,p) level even for the most problematic neutral stacked dimers. In the ionized systems, which are much more strongly bound, the effect of BSSE on the binding energy is even smaller. To quantify this effect, we computed the counterpoise correction for the stacked uracil dimer cation. The computed BSSE is 1.3 kcal/mol as estimated at the ωB97X-D level with the 6-311(+)G(d,p) basis set.

To obtain the standard thermodynamic quantities and the ZPE corrections, we performed vibrational analysis at the ωB97X-D/6-311(+)G**/EML(99,590) level for all complexes at the respective reoptimized geometries.

The electronic spectra of the dimer cations were obtained with IP-CCSD/6-31(+)G* at the cation and neutral geometries described above.

All open-shell DFT-D calculations employed the spin-unrestricted references. In these calculations, the spin contamination of the doublet Kohn−Sham determinant was low with typical $\langle S^2 \rangle$ values of 0.76−0.78.

All electrons were correlated in all the optimizations; in the single-point energy and spectral calculations the core electrons were frozen unless otherwise stated. The optimized geometries, corresponding reference energies, and frequencies are provided in the Supporting Information.

3. Results and Discussion

3.1. Molecular Orbital Framework. The character of the electronic states and the bonding patterns in ionized noncovalent dimers depend strongly on the relative orientation of the fragments.[19,21,35–37] Orbital overlap and electrostatic interactions are the most important factors determining the degree of hole delocalization, changes in bond strength due to ionization, and subsequent nuclear dynamics. When the two fragments are equivalent by symmetry, as in sandwich benzene dimers[35] or stacked C_2 nuclear base dimers,[19,21] the dimer states are derived from in-phase (bonding) and out-of-phase (antibonding) combination of the fragments MOs, and the initial hole is equally delocalized between the two fragments. The changes in IE due to dimerization depend on the orbital overlap; e.g., larger changes are observed for the states derived from ionizations of π orbitals.[19,21,35] Ionizations from antibonding orbitals increase the formal interfragment bond order and produce more tightly bound structures, whereas ionizations from the bonding orbitals result in dissociative states.

The orbital picture, changes in the vertical IEs, and initial hole delocalization are similar in symmetric hydrogen-bonded dimers; however, the ionization-induced dynamics is more complex and involves proton transfer.[19,20] The changes in the vertical IEs are smaller for most of the states due to a less favorable overlap. In dimers with nonequivalent fragments, the MOs (and, consequently, the initial hole) become more localized; however, changes in the IEs and wave functions can also be explained by overlap considerations within the DMO−LCFMO framework.[36,37] Finally, in nonsymmetric H-bonded dimers electrostatic interactions become more important than orbital overlap. For example, we observed large changes (0.4−0.7 eV) in the IEs and binding energies in some nonsymmetric hydrogen-bonded dimers of thymine and cytosine.[19,20] In these dimers, the hole localized on one of the fragments is stabilized by the dipole moment of the neutral fragment.

The electronic structure of the stacked and symmetric H-bonded uracil dimers at the respective neutral geometries was discussed in detail in ref 21. Below we focus on the T-shaped isomer. The principal difference between the

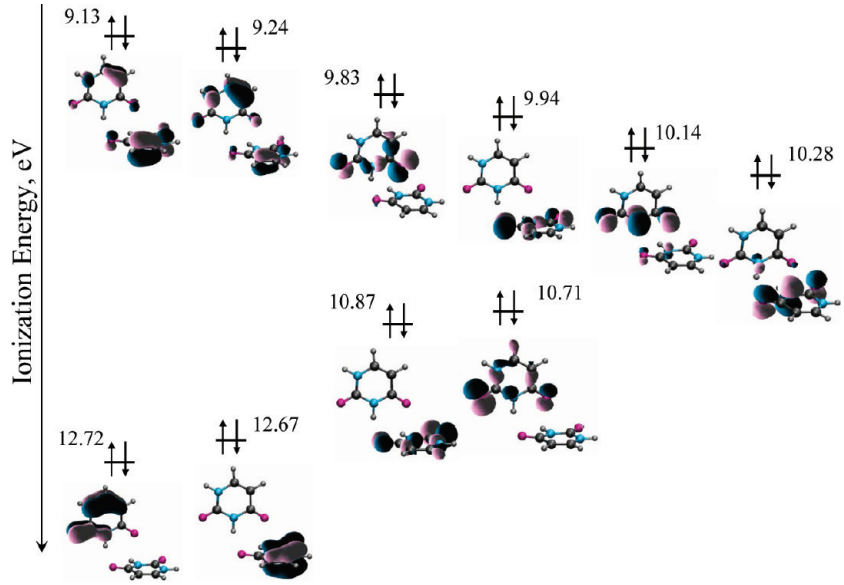

Figure 3. Ten lowest ionized states of the T-shaped uracil dimer at the neutral geometry calculated with IP-CCSD/6-311(+)G**.

T-shaped and the stacked or H-bonded structures is that in the former the two fragments are not equivalent by symmetry, which affects the electronic structure. The 10 lowest ionized states of the T-shaped uracil dimer and the corresponding MOs are presented in Figure 3. As in the stacked and H-bonded systems, the dimer MOs are formed from the MOs of the fragments, and the ionized states of the dimer correlate well with the states of the monomer (i.e., no mixing of the MOs of different character is observed). For example, the two highest lying MOs are the linear combinations of the π_{CC} MOs of the fragments. However, the MOs of the T-shaped dimer are more localized. For example, the lp(O) MO of the dimer is a localized lp(O) orbital of one of the fragments. For the four delocalized dimer orbitals [formed by the π_{CC} and lp(O) + lp(N) fragment orbitals] the distribution of electron density is also uneven. Owing to a less favorable overlap between the fragment MOs, the splitting between the pairs of ionized states in the T-shaped dimer is smaller. The largest splitting of 0.14 eV was observed for the dimer states derived from the π-like lp(O) + lp(N) fragment orbitals.

Despite less efficient overlap and smaller splittings between the pairs of states derived from the same FMOs, the absolute changes in the IEs in the T-shaped isomer are similar to those in the stacked dimer. For example, the lowest IE of this isomer is 9.13 eV. This value is red-shifted by 0.35, 0.22, and 0.01 eV relative to the first IE of the monomer and symmetric H-bonded and π-stacked dimers, respectively. This is similar to large changes in the IEs observed in the nonsymmetric H-bonded dimers of thymine and cytosine, where lowering of the IE was due to electrostatic stabilization of the localized hole by the dipole moment of the "neutral" fragment. The dipole moment of uracil is 4.19 D, which is comparable to the dipole moment of thymine (4.11 D).

3.2. Ionization-Induced Structural Changes: Equilibrium Geometries of the Uracil Dimer Cations. Ionization induces significant structural changes in the dimers, as can be seen from Figure 2. In the analysis below, we distinguish between the changes in the structures of the fragments (and compare those to ionization-induced changes in the monomer) and the interfragment relaxation. The definitions of the parameters are given in Figure 1, and their values are

Table 1. Values of the Optimized Structural Parameters (Å, deg) of the Fragments in the Stacked, H-Bonded, H-Transferred H-Bonded, and T-Shaped Uracil Dimer Cations[a]

param	SU_2^+	HU_2^+ (TS)	HU_2^+ (PT), F1	HU_2^+ (PT), F2	TU_2^+, F1	TU_2^+, F2	U^+
C_4-C_5	1.461, +0.010	1.461, +0.011	1.461, +0.011	1.458, +0.008	1.431, −0.026	1.475, +0.024	1.457, +0.011
C_5-C_6	1.367, +0.018	1.352, +0.002	1.407, +0.057	1.337, −0.013	1.353, +0.011	1.392, +0.050	1.386, +0.043
C_6-N_1	1.330, −0.038	1.352, −0.017	1.310, −0.059	1.391, +0.022	1.357, −0.012	1.324, −0.045	1.316, −0.049
N_1-C_2	1.405, +0.023	1.379, +0.012	1.411, +0.044	1.332, −0.035	1.389, −0.002	1.429, +0.044	1.433, +0.053
C_2-N_3	1.368, −0.014	1.349, −0.022	1.363, −0.008	1.331, −0.040	1.401, +0.023	1.377, −0.003	1.357, −0.017
N_3-C_4	1.384, −0.017	1.399, −0.008	1.400, −0.007	1.438, +0.031	1.365, −0.032	1.384, −0.007	1.387, −0.010
C_4-O_2	1.198, −0.024	1.190, −0.028	1.204, −0.014	1.194, −0.024	1.257, +0.041	1.206, −0.014	1.195, −0.020
C_2-O_1	1.182, −0.034	1.208, −0.023	1.216, −0.015	1.287, +0.056	1.195, −0.012	1.190, −0.017	1.178, −0.034
$C_4-C_5-C_6$	119.3, −0.5	119.5, −0.1	119.4, −0.2	120.4, +0.7	118.4, −1.1	119.5, +0.3	119.7, −0.1
$C_5-C_6-N_1$	121.0, −0.9	121.1, −1.5	123.1, +0.6	121.8, −0.7	121.9, +0.2	120.1, −1.8	119.4, −2.6
$C_6-N_1-C_2$	124.3, +0.8	123.4, +0.9	120.1, −2.4	121.0, −1.5	123.7, +0.2	124.9, +1.4	125.5, +2.0
$N_1-C_2-N_3$	113.8, +0.8	115.4, +1.1	118.2, +3.9	118.8, +4.5	112.9, −0.6	113.5, +0.4	113.6, +0.8
$C_2-N_3-C_4$	126.9, −1.2	126.3, −1.8	125.5, −2.6	125.5, −2.6	126.2, −1.1	127.0, −0.4	126.2, −2.4
$N_3-C_4-C_5$	114.7, +1.3	114.3, +1.4	113.7, +0.8	112.5, −0.4	116.9, +2.5	114.7, +0.2	115.7, +2.4
Σ(angles)	719.9, +0.3				720.0, +0.0	719.7, +0.1	720.0, +0.0

[a] The differences (Å, deg) with respect to the equilibrium geometry of the respective neutral complex are also given, showing the ionization-induced changes in the geometry. See Figure 1 for the definitions of the parameters.

Table 2. Values of the Interfragment Structural Parameters (Å, deg) of the Stacked, H-Bonded, H-Transferred H-Bonded, and T-Shaped Uracil Dimer Cations[a]

SU_2^+		HU_2^+ (TS)		HU_2^+ (PT)		TU_2^+	
C_5-C_6	3.299 (−0.451)	O_1-H_1	1.828 (+0.053)	O_1-H_1	1.749 (−0.026)	H_2-O_2	2.000 (+0.072)
O_2-N_1	3.116 (−0.175)	O_2-H_1	1.828 (+0.053)	O_2-H_1	1.018 (−0.757)	O_2-C_5	2.178 (−1.099)
						O_2-C_6	2.701 (−0.950)
α	18.4 (+5.6)						
d	3.51 (+0.34)						

[a] The differences (Å, deg) with respect to the equilibrium geometry of the respective neutral complexes are given in parentheses. See Figure 1 for the definitions of the parameters.

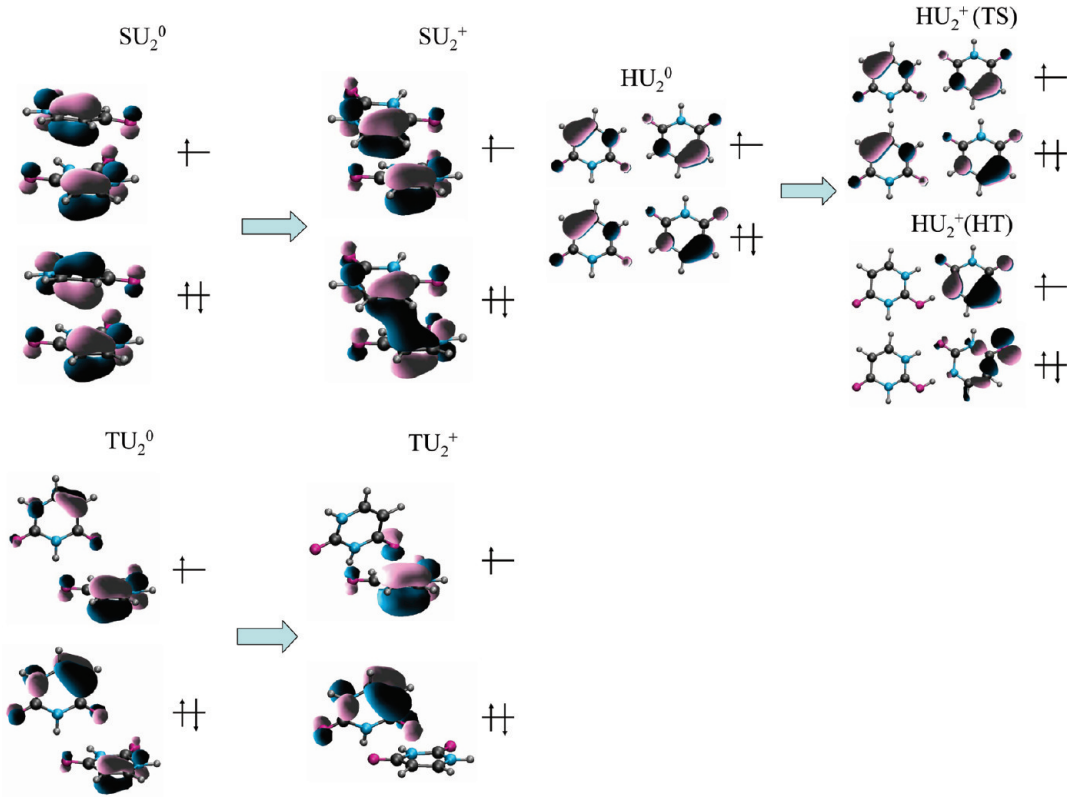

Figure 4. Two highest occupied MOs of the three isomers of the uracil dimer at the neutral and cation geometries.

summarized in Tables 1 and 2. Only the symmetry-unique parameters are given.

First, let us consider the effect of ionization on the intrafragment parameters (see Table 1) and compare the monomer and the symmetric dimer cation data. The magnitude of relaxation in the monomer is larger than in the stacked and H-bonded dimers. For instance, the C_5-C_6 bond increases by 0.043 Å in the monomer versus 0.018 and 0.002 Å in the stacked and H-bonded dimers, respectively. The sign of the change in the monomer and the symmetric dimers is the same for all the parameters, which is consistent with the DMO−LCFMO picture. The magnitude of the changes is smaller in the dimers because the hole is delocalized over the two fragments.

In the nonsymmetric dimers, the fragments are not equivalent and the orbital picture is more complicated. The hole is distributed unevenly between the two fragments, such that the positive charge is localized on one of them. Comparing the data presented in Table 7 for the H-bonded proton-transferred and the T-shaped dimer cations with those of the monomer, we observe that the structural changes of fragment 1 (F1) of HU_2^+ (PT), fragment 2 (F2) of TU_2^+, and the monomer cation are very similar. For instance, the C_5-C_6 bond increases by 0.057, 0.050, and 0.043 Å in fragment 1 of HU_2^+ (PT), fragment 2 of TU_2^+, and the monomer cation, respectively. Thus, one of the fragments in nonsymmetric dimers relaxes similarly to the monomer cation, while the other adjusts accordingly. This is similar to what is found in the T-shaped benzene dimer.[36]

The ionization-induced changes in the interfragment parameters (given in Table 2) and the MOs (shown in Figure 4) are consistent with the DMO−LCFMO predictions: the fragments adjust their relative orientation to maximize the overlap between their HOMOs (π_{CC}).

The change in the MOs is illustrated in Figure 4 depicting HOMOs at the neutral and the cation geometries. In the stacked dimer, the two π_{CC} FMOs give rise to efficient overlap, lending a partial covalent character to the ionized dimer. In the T-shaped dimer, the changes in the HOMO are different. Upon relaxation, the hole becomes more localized on the lower fragment, and the only contribution to the overlap is due to the oxygen lone pair of the top fragment pointing toward the π_{CC} MO of the lower fragment.

Table 3. Total (E_{tot}, hartrees) and Dissociation (D_e, kcal/mol) Energies of the Four Isomers of the Uracil Dimer in the Neutral and Ionized States Computed by CCSD/IP-CCSD with 6-311(+)G** [a]

complex	E_{tot}^{CCSD}	D_e^{CCSD}	ΔE^{CCSD}
U^0	−413.882 346		
U^+	−413.542 383		−5.41
UH^+	−414.209 422		
$(U-H)^0$	−413.212 558		
SU_2^0	−827.782 419	11.1	
SU_2^+	−827.456 874	20.2	−6.48
HU_2^0	−827.793 226	17.9	
HU_2^+ (TS)[b]	−827.450 565	16.2	−0.64
HU_2^+ (PT)[c]	−827.475 648	32.0/33.7	
TU_2^0	−827.779 232	9.1	
TU_2^+	−827.463 991	24.6	−12.71

[a] The relevant total energies of the uracil monomer are also given. The relaxation energies (ΔE, kcal/mol) defined as the difference in the total energies of the cation at the neutral and relaxed cation geometries are also shown. For HU_2^+ (PT) dissociation energies corresponding to the $U^0 + U^+/(U-H)^0 + UH^+$ channels are given. [b] Transition state. [c] Proton-transferred structure, UH^+ (U−H).

The magnitude of the relaxation is quantified by Table 3, which presents the differences in the total energies between the relaxed and vertical structures of the dimer cations calculated by EOM-IP-CCSD/6-311(+)G**. For the T-shaped, stacked, and H-bonded isomers, ΔE^{CCSD} is −12.71, −6.48, and −0.64 kcal/mol, respectively. Such a large relaxation effect in the T-shaped cation is somewhat surprising, as from Figure 4 the FMOs overlap more efficiently in the stacked dimer. The reason is the electrostatic interaction of the lone pair on the oxygen of fragment 1 and the hole on fragment 2, which stabilizes the T-shaped structure.[19]

The interfragment parameters presented in Table 2 are consistent with the MO changes. In the stacked dimer cation, the fragments slide with respect to each other, so the overlap of FMOs centered on the C_5, C_6, N_1, and O_2 atoms increases (see Figure 4). The C_5-C_6 and O_2-N_1 distances decrease by 0.451 and 0.175 Å, respectively. Surprisingly, the distance between the centers-of-masses of the fragments increases by 0.34 Å in the cation with respect to the neutral. This illustrates that the average geometric parameters in polyatomic systems can be misleading.

In the T-shaped cation, the fragments move to minimize the distance between the lone pair on O_2 of the top fragment and the π_{CC} MO of the bottom fragment. The characteristic parameters in this case are the O_2-C_5 and O_2-C_6 distances, which decrease by 1.099 and 0.950 Å, respectively.

In the symmetric H-bonded dimer, the structural changes and, consequently, relaxation energy are small. As one can see from Figure 4, there are also no significant changes in the MOs upon relaxation due to unfavorable orbital overlap. Moreover, this symmetric structure is a transition state, as shown by the vibrational analysis discussed later. Much larger stabilization is achieved by a proton transfer, which lowers the total energy by 15.7 kcal/mol, making the proton-transferred H-bonded isomer the lowest energy structure on the cation's PES.

3.3. Binding Energies of the Neutral and Ionized Uracil Dimers: Potential and Free Energy Calculations. *3.3.1. Potential Energy Profile.* Figures 5 and 6 present the relative ordering and binding energies of the neutral and ionized uracil dimers calculated by IP-CCSD and ωB97X-D with the 6-311(+)G** basis. In the neutral, the symmetric H-bonded uracil dimer is the minimum energy isomer, with the stacked and T-shaped dimers lying 6.8 and 8.8 kcal/mol higher in energy. Excluding the proton-transferred dimer, the lowest energy cation structure is the T-shaped one. The energy spacing between the T-shaped and the stacked and H-bonded cations is 4.4 and 8.4 kcal/mol, respectively. Upon proton transfer the total energy of the H-bonded cation is lowered by 15.8 kcal/mol, so that it lies 7.4 kcal/mol below that of the T-shaped cation.

The calculated binding energies for the H-bonded, stacked, and T-shaped neutral dimers are 17.9, 11.1, and 9.1 kcal/mol, respectively. The DFT-D and CCSD values are within 1 kcal/mol of each other. The D_e values for the stacked and

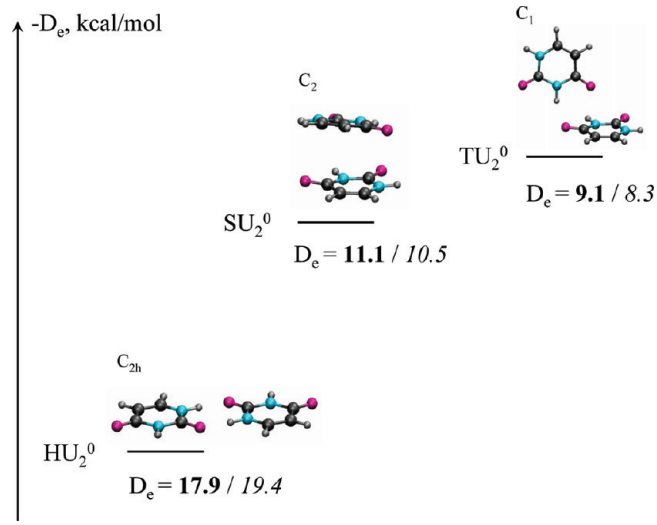

Figure 5. Binding energies (kcal/mol) of the three isomers of the neutral uracil dimer calculated at two levels of theory: CCSD/6-311(+)G** (shown in bold) and ωB97X-D/6-311(+)G**/EML(99,590) (shown in italic).

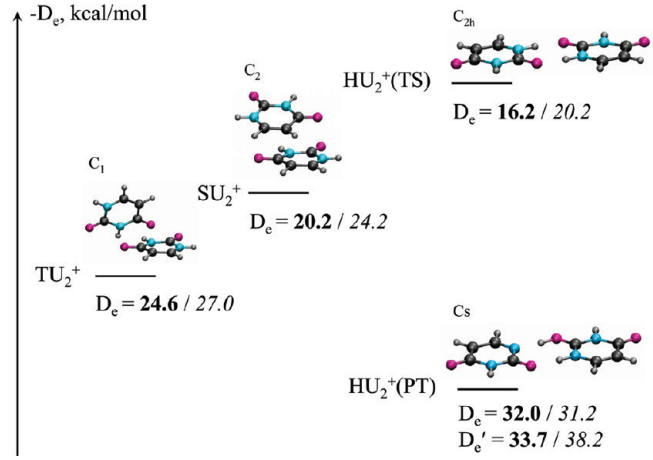

Figure 6. Binding energies (kcal/mol) of the three isomers of the uracil dimer cation calculated at two levels of theory: IP-CCSD/6-311(+)G** (shown in bold) and ωB97X-D/6-311(+)G**/EML(99,590) (shown in italic). For the proton-transferred H-bonded uracil dimer cation, the binding energies corresponding to the two dissociation limits are presented.

Table 4. Dissociation Energies (kcal/mol) and Standard Thermodynamic Quantities of the Neutral and the Cation Uracil Dimers Calculated at the ωB97X-D/6-311(+)G**/EML(99,590) Level[a]

reaction	D_e	D_0	$\Delta H°$, kcal/mol	$\Delta S°$, cal/(mol K)	$\Delta G°$, kcal/mol
$SU_2^0 \rightarrow U^0 + U^0$	10.5	9.8	8.4	31.5	−1.0
$SU_2^+ \rightarrow U^0 + U^+$	24.4	22.7	20.9	40.4	8.8
$HU_2^0 \rightarrow U^0 + U^0$	19.4	18.2	16.8	38.1	5.4
HU_2^+ (TS) $\rightarrow U^0 + U^+$	20.2	21.8	23.2	40.5	11.1
HU_2^+ (TS) $\rightarrow HU_2^+$ (PT)	11.0	13.1	−8.8	2.7	−9.6
HU_2^+ (PT) $\rightarrow U^0 + U^+$	31.2	30.6	−0.7	37.7	18.7
HU_2^+ (PT) $\rightarrow (U - H)^0 + UH^+$	38.2	37.0	−1.3	38.6	24.2
$TU_2^0 \rightarrow U^0 + U^0$	8.3	7.6	6.2	29.6	−2.6
$TU_2^+ \rightarrow U^0 + U^+$	27.0	25.1	23.0	38.8	11.4

[a] For the proton-transferred H-bonded cation the values corresponding to the two different dissociation limits are given.

H-bonded isomers are also in good agreement with the recent CCSD(T)/CBS values of 20.4 and 9.7 kcal/mol from ref 62.

Note that the interaction of the fragments in the neutral uracil dimers is much stronger than in the benzene dimers, where the typical interaction energies lie in the range of 1.5−3.0 kcal/mol for all isomers.[63,64] The binding energies increase upon ionization, in agreement with the DMO−LCFMO predictions. In the T-shaped, stacked, and symmetric H-bonded cations the fragments are bound by 24.6, 20.2, and 16.2 kcal/mol, respectively. For comparison, in the benzene dimer cation the binding energies are 20 and 12 kcal/mol for the sandwich and T-shaped isomers, respectively.[35,36] However, the strongest interaction is observed in the proton-transferred H-bonded cation, where the binding energy corresponding to the $U^0 + U^+$ dissociation channel is 32.0 kcal/mol [this channel lies 1.8 kcal/mol below an alternative $(U-H)^0 + UH^+$ channel].

In conclusion, when the uracil dimer is ionized, the interaction between the fragments increases almost 2-fold for the stacked and H-bonded isomers and more than 2-fold for the T-shaped isomer. Such a strong increase in interaction in the T-shaped structure is very different from that of the benzene dimer cation and can be explained by electrostatic interactions rather than orbital overlap considerations. The H-bonded isomer is stabilized by the proton transfer.

3.3.2. Free Energy Profile. It has been argued that the entropy contribution to the stability can be important in the nucleobase dimer systems favoring stacked isomers over H-bonded isomers.[65] Thus, we performed vibrational analysis using ωB97X-D. Moreover, we wanted to quantify the zero-point energy (ZPE) corrections to the dissociation energies. The calculated dissociation energies and the standard thermodynamic quantities for the dissociation of the neutral and the ionized dimers are given in Table 4.

Among the neutral uracil dimers, only the H-bonded isomer is predicted to be stable under the standard conditions ($\Delta G° = 5.4$ kcal/mol). Standard Gibbs free energies, $\Delta G°$, of the stacked and T-shaped isomers are −1.0 and −2.6 kcal/mol, respectively. The data in Table 2 show that the entropy contribution is similar for all three isomers: $\Delta S°$ of dissociation is 31.5, 38.1, and 29.6 cal/(mol K) for the stacked, H-bonded, and T-shaped isomers, respectively. However, more appropriate treatment including anharmonicities may discriminate between the isomers more. The enthalpy contribution is different: for the H-bonded uracil dimer the enthalpy of dissociation is 16.8 kcal/mol, whereas the corresponding values for the stacked and T-shaped isomers are 8.4 and 6.2 kcal/mol, respectively.

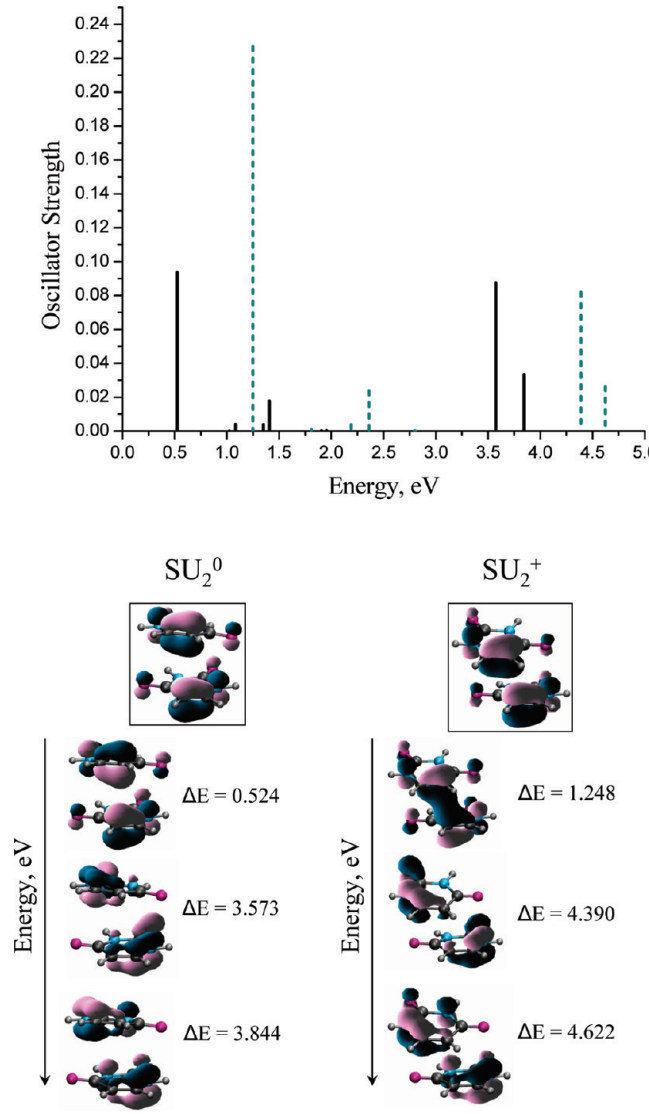

Figure 7. Electronic spectra (top panel) of the stacked uracil dimer cation at the neutral (solid black) and the cation (dashed blue) geometries calculated with IP-CCSD/6-31(+)G* and the electronic states corresponding to the three most intense transitions (bottom panel).

Unlike neutrals, all of the dimer cation isomers are stable under the standard conditions. The most stable isomer is the proton-transferred H-bonded cation with a $\Delta G°$ of 18.7 kcal/mol. In order of decreasing stability, the proton-transferred

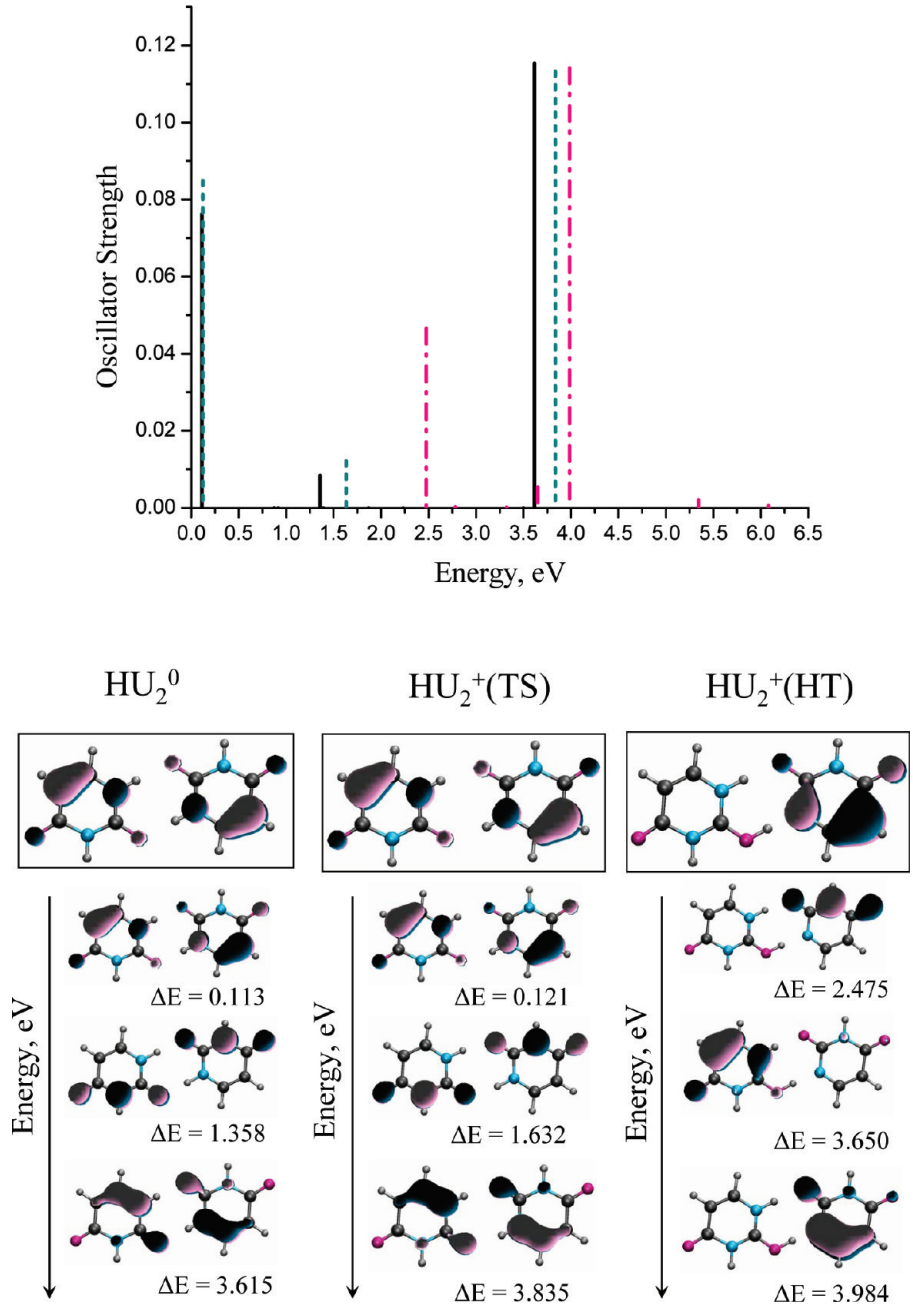

Figure 8. Electronic spectra (top panel) of the H-bonded uracil dimer cation at the neutral (solid black), symmetric transition state (dashed blue), and proton-transferred cation (dashed−dotted pink) geometries calculated with IP-CCSD/6-31(+)G* and the electronic states corresponding to the three most intense transitions (bottom panel).

dimer is followed by the T-shaped, symmetric H-bonded (TS), and stacked isomers. Again, the $\Delta S°$ values are very close for all of the isomers, being 40.4, 40.5, 37.7, and 38.8 cal/(mol K) for SU_2^+, HU_2^+ (TS), HU_2^+ (PT), and TU_2^+, respectively, whereas the $\Delta H°$ contributions are different.

Thus, we conclude that the enthalpy determines the relative stability of the neutral and ionized uracil dimers to a high degree, while the entropy contribution has a less pronounced effect.

Lastly, the ZPE corrections lower the dissociation energy estimates by 0.6−1.9 kcal/mol for all the neutral and ionized dimers, except for the symmetric H-bonded dimer. In the symmetric H-bonded dimer, the ZPE correction has the opposite sign and increases the dissociation energy by 1.6 kcal/mol, because this structure is a transition state with one imaginary frequency.

3.4. Electronic Spectra of the Uracil Dimer Cations. This section presents the calculated electronic spectra of the uracil dimer cations. The spectra of the stacked and H-bonded isomers at the geometry of the neutral were described in a detail in previous work;[21] therefore, we focus on the effect of geometry relaxation on the spectroscopic properties. For the H-bonded dimer, we present the spectra of both the symmetric (TS) and the proton-transferred structures.

Figures 7−9 present the electronic spectra of the stacked, H-bonded, and T-shaped uracil dimers, respectively, calculated by IP-CCSD/6-31(+)G* at the neutral and the cation geometries. Figures 7−9 also show the character of the

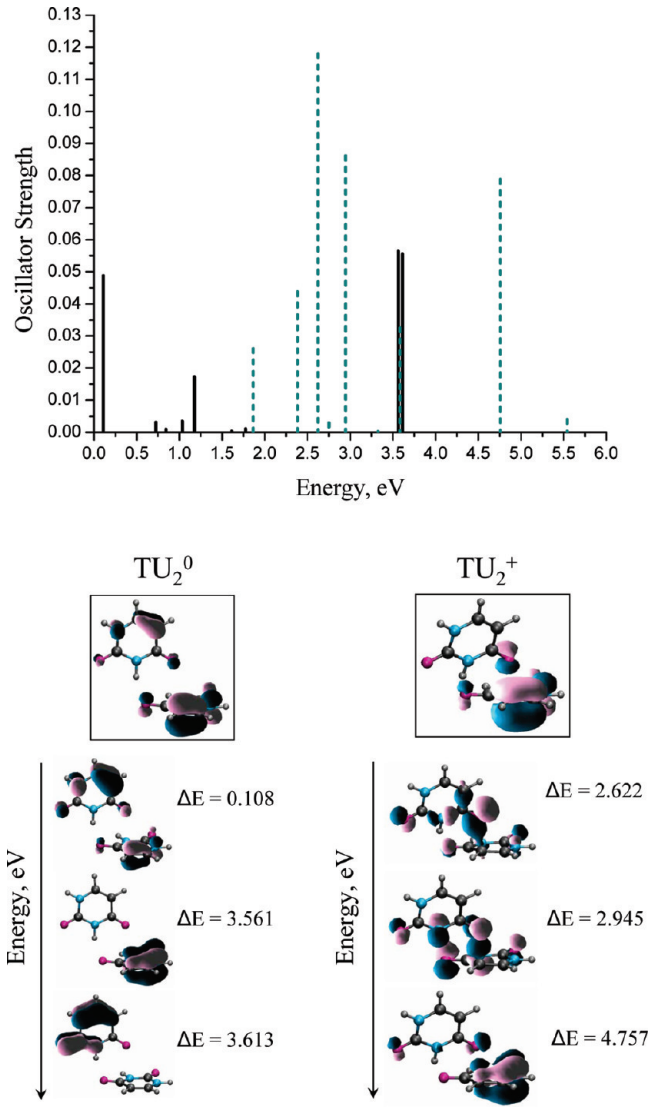

Figure 9. Electronic spectra (top panel) of the T-shaped uracil dimer cation at the neutral (solid black) and the cation (dashed blue) geometries calculated with IP-CCSD/6-31(+)G* and the electronic states corresponding to the three most intense transitions (bottom panel).

electronic states corresponding to the three most intense transitions in each spectrum. The transition energies, transition dipole moments, and oscillator strengths are provided in Tables 5−8.

The spectrum of the stacked dimer at the neutral geometry is dominated by three intense lines at 0.5, 3.5, and 3.8 eV (see Figure 7). The first peak is the CR band, which is unique to the dimer, while the others are the LEs between the states of the cation with the various π-orbitals singly occupied. Upon geometric relaxation, the spectrum shifts to higher energies by approximately 0.8 eV, so the lines appear at 1.2, 4.4, and 4.6 eV. The intensity of the charge resonance band increases more than 2-fold upon relaxation.

The H-bonded dimer cation spectrum at the geometry of the neutral (see Figure 8) features two intense lines at 0.1 and 3.6 eV and a small peak at 1.3 eV. As in the stacked cation, these lines are the CR band and two LEs corresponding to the transition between the π-orbitals of the cation (see Figure 8). The CR band is less intense than in the stacked

Table 5. Excitation Energies (ΔE, eV), Transition Dipole Moments ($\langle\mu^2\rangle$, au), and Oscillator Strengths (f) of the Stacked Dimer Cation at the Geometry of the Neutral and Cation (IP-CCSD/6-31(+)G*)

	neutral			cation		
transition	ΔE	$\langle\mu^2\rangle$	f	ΔE	$\langle\mu^2\rangle$	f
$X^2B \rightarrow 1^2A$	0.524	7.2918	0.0935	1.248	7.4212	0.2269
$X^2B \rightarrow 2^2B$	1.023	0.0028	0.0000	1.799	0.0010	0.0000
$X^2B \rightarrow 2^2A$	1.081	0.1503	0.0040	1.809	0.0197	0.0009
$X^2B \rightarrow 3^2B$	1.349	0.1141	0.0038	2.190	0.0709	0.0038
$X^2B \rightarrow 3^2A$	1.406	0.5171	0.0178	2.362	0.4090	0.0237
$X^2B \rightarrow 4^2B$	1.906	0.0024	0.0001	2.798	0.0010	0.0000
$X^2B \rightarrow 4^2A$	1.952	0.0053	0.0003	2.800	0.0016	0.0001
$X^2B \rightarrow 5^2B$	3.573	0.3531	0.0333	4.390	0.7613	0.0819
$X^2B \rightarrow 5^2A$	3.844	0.9990	0.0875	4.622	0.2323	0.0263

Table 6. Excitation Energies (ΔE, eV), Transition Dipole Moments ($\langle\mu^2\rangle$, au), and Oscillator Strengths (f) of the Symmetric H-Bonded Dimer Cation at the Geometry of the Neutral and Cation (IP-CCSD/6-31(+)G*)

	neutral			cation		
transition	ΔE	$\langle\mu^2\rangle$	f	ΔE	$\langle\mu^2\rangle$	f
$X^2A_u \rightarrow 1^2B_g$	0.113	27.4607	0.0763	0.121	28.7406	0.0849
$X^2A_u \rightarrow 1^2B_u$	0.871	0.0000	0.0000	1.064	0.0000	0.0000
$X^2A_u \rightarrow 1^2A_g$	0.915	0.0003	0.0000	1.123	0.0003	0.0000
$X^2A_u \rightarrow 2^2B_g$	1.358	0.2527	0.0084	1.632	0.3048	0.0122
$X^2A_u \rightarrow 2^2A_u$	1.391	0.0000	0.0000	1.683	0.0000	0.0000
$X^2A_u \rightarrow 2^2B_u$	1.867	0.0000	0.0000	1.954	0.0000	0.0000
$X^2A_u \rightarrow 2^2A_g$	2.232	0.0000	0.0000	2.381	0.0000	0.0000
$X^2A_u \rightarrow 3^2A_u$	3.501	0.0000	0.0000	3.740	0.0000	0.0000
$X^2A_u \rightarrow 3^2B_g$	3.615	1.3026	0.1154	3.835	1.2053	0.1133

Table 7. Excitation Energies (ΔE, eV), Transition Dipole Moments ($\langle\mu^2\rangle$, au), and Oscillator Strengths (f) of the H-Bonded Dimer Cation at the Optimized Proton-Transferred Geometry (IP-CCSD/6-31(+)G*)

transition	ΔE	$\langle\mu^2\rangle$	f
$X^2A'' \rightarrow 1^2A'$	1.702	0.0004	0.0000
$X^2A'' \rightarrow 2^2A''$	2.475	0.7690	0.0466
$X^2A'' \rightarrow 2^2A'$	2.782	0.0040	0.0003
$X^2A'' \rightarrow 3^2A'$	3.325	0.0024	0.0002
$X^2A'' \rightarrow 3^2A''$	3.650	0.0605	0.0054
$X^2A'' \rightarrow 4^2A''$	3.984	1.1704	0.1142
$X^2A'' \rightarrow 4^2A'$	4.493	0.0001	0.0000
$X^2A'' \rightarrow 5^2A''$	5.343	0.0162	0.0021
$X^2A'' \rightarrow 5^2A'$	6.082	0.0039	0.0006

cation, and the most intense transition is the LE at 3.6 eV. The spectrum at the transition-state structure exhibits only minor differences, i.e., 0.1 eV blue shifts in the peak positions with the intensities remaining the same. However, the spectrum and the character of the states change dramatically upon proton transfer. A new band appears at 2.5 eV. The localized character of the states and C_s symmetry make the proton-transferred H-bonded cation spectrum very similar to that of the uracil cation.

In the T-shaped cation spectrum at the neutral geometry, the CR and the two intense LE transitions appear at 0.1, 3.5, and 3.6 eV (see Figure 9). The spectrum is very similar to that of the H-bonded isomer at the neutral geometry. As in the stacked and H-bonded cations, the transitions between the π-like orbitals are the most intense. However, the character of the states is different: the states are more

Table 8. Excitation Energies (ΔE, eV), Transition Dipole Moments ($\langle\mu^2\rangle$, au), and Oscillator Strengths (f) of the T-Shaped Dimer Cation at the Geometry of the Neutral and Cation (IP-CCSD/6-31(+)G*)

	neutral			cation		
transition	ΔE	$\langle\mu^2\rangle$	f	ΔE	$\langle\mu^2\rangle$	f
$X^2A_1 \rightarrow 2^2A_1$	0.108	18.4996	0.0488	1.866	0.5715	0.0261
$X^2A_1 \rightarrow 3^2A_1$	0.725	0.1761	0.0031	2.384	0.7506	0.0438
$X^2A_1 \rightarrow 4^2A_1$	0.841	0.0436	0.0009	2.622	1.8376	0.1180
$X^2A_1 \rightarrow 5^2A_1$	1.031	0.1376	0.0035	2.750	0.0428	0.0029
$X^2A_1 \rightarrow 6^2A_1$	1.176	0.5961	0.0172	2.945	1.1927	0.0861
$X^2A_1 \rightarrow 7^2A_1$	1.609	0.0095	0.0004	3.324	0.0042	0.0003
$X^2A_1 \rightarrow 8^2A_1$	1.776	0.0261	0.0011	3.584	0.3711	0.0326
$X^2A_1 \rightarrow 9^2A_1$	3.561	0.6475	0.0565	4.757	0.6759	0.0788
$X^2A_1 \rightarrow 10^2A_1$	3.613	0.6276	0.0555	5.539	0.0295	0.0040

localized. Upon relaxation, the spectrum changes completely, as does the character of the states. The maximum intensity increases 2.5 times, and new intense lines appear in the 1.7−3.0 and 4.5−5.0 eV regions. The orbital picture is now much more complex: the DMOs become combinations of several FMOs. Thus, the electronic transitions can no longer be described as CR or LE excitations. The most intense bands correspond to the transitions between the cation states with the π_{CC} orbital and the lp(O) orbital singly occupied and are of charge-transfer character.

To summarize, the three isomers have distinctly different spectra, which can be used to distinguish between them experimentally. Moreover, significant changes upon relaxation may be exploited to monitor ionization-induced dynamics in a pump−probe experiment. Immediately upon ionization, the isomers will exhibit intense lines in three regions: 0.0−0.7, 1−1.5, and 3.0−4.0 eV. While the spectra of the H-bonded and T-shaped dimers at the neutral geometry are similar, the stacked cation can be distinguished by the two peaks of moderate intensity in the 0.5−0.7 and 3.5−4.0 eV regions. Upon relaxation, the most intense CR band of the stacked isomer shifts to 1.2 eV and acquires additional intensity. The relaxation of the T-shaped cation manifests itself by significant growth of intensity in the 2.5−3.0 eV region. The hydrogen-bonded complex is more difficult to distinguish because of the overlap of its spectral lines with the stacked and T-shaped spectra. Still, the signature of proton transfer is the 0.3−0.4 eV blue shift of the intense transition in the 3.5−4.0 eV region.

4. Conclusions

We characterized the electronic structure of three representative isomers of the ionized uracil dimers: H-bonded, stacked, and T-shaped. The interactions between the fragments lower the vertical IEs by 0.13−0.35 eV, the largest drop in IE being observed for the stacked and T-shaped isomers. Interestingly, the character of the ionized states and the origin of the IE change are different in these two isomers. In the stacked dimer, the hole is delocalized between the two fragments and orbital overlap determines the change in the IE. In the T-shaped isomer, the hole is localized and the change in the IE is due to electrostatic interactions between the "ionized" and the "spectator" fragments. The change in the IE for the symmetric H-bonded dimer is small, because neither overlap nor electrostatic interactions can stabilize the hole; however, larger changes are expected for the nonsymmetric H-bonded dimers.[19]

The geometric relaxation is also different for the three isomers. The stacked isomer relaxes to a tighter structure with more efficient overlap between the FMOs, and the hole remains delocalized between the fragments. The H-bonded isomer undergoes proton transfer, forming the lowest energy structure on the cation's surface in which the charge and the unpaired electron are localized on different moieties. Finally, the T-shaped dimer relaxes to the structure with the localized hole. The respective binding energies of the cation isomers are 22.7, 37.0, and 25.1 kcal/mol.

Finally, we characterized the electronic spectra of the cations at the neutral and the relaxed geometries. At the neutral geometry, the H-bonded and stacked isomers feature intense CR bands at 0.1 and 0.5 eV, respectively. The CR band in the T-shaped isomer is less intense and appears at the same energy as in the H-bonded dimer (0.11 eV). For all three isomers, the spectra change dramatically upon relaxation. In the stacked isomer, the intense CR band shifts to higher energies (i.e., from 0.5 to 1.3 eV) and becomes even more intense. In the H-bonded isomer, the CR bands (present at the neutral geometry at 0.1 eV) disappear upon proton transfer and the spectrum becomes very similar to that of the monomer. In the T-shaped isomer, new intense lines corresponding to charge-transfer transitions develop at 2.5−3.0 eV. Thus, the spectral evolution in these isomers is rather different, which may be exploited for their experimental determination.

Acknowledgment. We are grateful to Dr. Ksenia Bravaya for her insightful remarks and critical reading of the paper. This work was conducted in the framework of the iOpenShell Center for Computational Studies of Electronic Structure and Spectroscopy of Open-Shell and Electronically Excited Species (iopenshell.usc.edu) supported by the National Science Foundation through Grants CRIF:CRF CHE-0625419+0624602+0625237 and CHE-0616271.

Appendix: Performance of ωB97X-D for the Structures and Energetics of Noncovalent Neutral and Ionized Dimers

Self-interaction-corrected functionals provide more a reliable (although not fully satisfactory) description of the ionized noncovalent dimers than the standard functionals. To investigate the performance of the ωB97X-D functional[55] as an inexpensive alternative to more reliable wave function methods, we benchmarked this functional using the stacked uracil isomer. We compared the intra and interfragment structural parameters of the ωB97X-D/6-311(+)G**-optimized geometries of the neutral and the cation with the best available geometries. For the neutral system, the geometry from the S22 set of Hobza and co-workers was used as a benchmark.[59] For the cation, we compared against the IP-CISD/6-31(+)G*-optimized geometry. The average absolute errors and the standard deviations for the bond lengths and angles in the DFT-D-optimized geometries were calculated. In the neutral, the average absolute error and the standard

deviation for the bond lengths were 0.004 and 0.003 Å, respectively; the average absolute error and standard deviation for the angles were 0.247 and 0.182°. In the cation, the corresponding values were 0.010 and 0.005 Å and 0.377 and 0.233°. As for the interfragment parameters, in the neutral the DFT-D parameters (C_5-C_6 and O_2-N_1) differ by less than 0.05 Å from the geometry from the S22 set, while in the cation DFT-D overestimated them by 0.15 Å relative to the IP-CISD/6-31(+)G* value. Given the tendency of IP-CISD to overestimate the interfragment distances in weakly bound systems by 0.2−0.3 Å (as compared to the more accurate IP-CCSD),[51] the DFT-D geometry of the cation may be more accurate than the IP-CISD geometry. We conclude that the ωB97X-D structures are fairly accurate, which validates the use of this method for geometry optimizations of the ionized dimers.

To assess the performance of the ωB97X-D functional for the energetics, we computed the dissociation energies for all isomers of the neutral and cation dimers and compared them to the IP-CCSD/6-311(+)G** values. The results are summarized in Figures 4 and 5. ωB97X-D predicts the correct relative ordering of the neutral and cation isomers. Quantitatively, the DFT-D errors in dissociation energies with respect to the IP-CCSD values are in the 1−2 kcal/mol range for the neutral dimers and in the 1−5 kcal/mol range for the cations. The errors in D_e are nonsystematic. Therefore, DFT-D with the ωB97X-D functional provides a correct qualitative picture for the energetics; the quantitative predictions are of moderate accuracy, so a more reliable approach should be employed.

Supporting Information Available: Optimized geometries, corresponding reference energies, and frequencies (TXT). This material is available free of charge via the Internet at http://pubs.acs.org.

References

(1) Nácuteuñez, M. E.; Hall, D. B.; Barton, J. K. *Chem. Biol.* **1999**, *6*, 85.

(2) Henderson, P. T.; Jones, D.; Hampikian, G.; Kan, Y.; Schuster, G. B. *Proc. Natl. Acad. Sci. U.S.A.* **1999**, *96*, 8353.

(3) Lewis, F. D.; Letsinger, R. L.; Wasielewski, M. R. *Acc. Chem. Res.* **2001**, *34*, 159.

(4) Candeias, L. P.; Steenken, S. *J. Am. Chem. Soc.* **1989**, *111*, 1094.

(5) Hutter, M.; Clark, T. *J. Am. Chem. Soc.* **1996**, *118*, 7574–7577.

(6) Ghosh, A. K.; Schuster, G. B. *J. Am. Chem. Soc.* **2006**, *128*, 4172.

(7) de Vries, M. S. In *Radiation Induced Molecular Phenomena in Nucleic Acids*; Shukla, M., Leszczynski, J., Eds.; Springer: Berlin, 2008; p 323.

(8) Dougherty, D.; Wittel, K.; Meeks, J.; McGlynn, S. P. *J. Am. Chem. Soc.* **1976**, *98*, 3815.

(9) Urano, S.; Yang, X.; LeBrenton, P. R. *J. Mol. Struct.* **1989**, *214*, 315.

(10) Lauer, G.; Schäfer, W.; Schweig, A. *Tetrahedron Lett.* **1975**, *16*, 3939.

(11) Yu, C.; O'Donnel, T. J.; LeBreton, P. R. *J. Phys. Chem.* **1981**, *85*, 3851.

(12) Kim, S. K.; Lee, W.; Herschbach, D. R. *J. Phys. Chem.* **1996**, *100*, 7933.

(13) Satzger, H.; Townsend, D.; Stolow, A. *Chem. Phys. Lett.* **2006**, *430*, 144.

(14) Belau, L.; Wilson, K. R.; Leone, S. R.; Ahmed, M. *J. Phys. Chem. A* **2007**, *111*, 7562.

(15) Cauët, E.; Dehareng, D.; Liévin, J. *J. Phys. Chem. A* **2006**, *110*, 9200.

(16) Roca-Sanjuán, D.; Rubio, M.; Merchán, M.; Serrano-Andrés, L. *J. Chem. Phys.* **2006**, *125*, 084302.

(17) Cauët, E.; Liévin, J. *Adv. Quantum Chem.* **2007**, *52*, 121.

(18) Hudock, H. R.; Levine, B. G.; Thompson, A. L.; Satzger, H.; Townsend, D.; Gador, N.; Ulrich, S.; Stolow, A.; Martínez, T. J. *J. Phys. Chem. A* **2007**, *111*, 8500.

(19) Bravaya, K. B. ; Kostko, O. ; Ahmed, M. ; Krylov, A. I. *Phys. Chem. Chem. Phys.*, in press.

(20) Kostko, O.; Bravaya, K. B.; Krylov, A. I.; Ahmed, M. *Phys. Chem. Chem. Phys.*, submitted for publication.

(21) Golubeva, A. A.; Krylov, A. I. *Phys. Chem. Chem. Phys.* **2009**, *11*, 1303.

(22) Colson, A.-O.; Besler, B.; Sevilla, M. D. *J. Phys. Chem.* **1992**, *96*, 9787.

(23) Colson, A.-O.; Besler, B.; Sevilla, M. D. *J. Phys. Chem.* **1993**, *97*, 13852.

(24) Sugiyama, H.; Saito, I. *J. Am. Chem. Soc.* **1996**, *118*, 7063.

(25) Prat, F.; Houk, K. N.; Foote, C. S. *J. Am. Chem. Soc.* **1998**, *120*, 845.

(26) Schumm, S.; Prévost, M.; Garcia-Fresnadillo, D.; Lentzen, O.; Moucheron, C.; Krisch-De Mesmaeker, A. *J. Phys. Chem. B* **2002**, *106*, 2763.

(27) Roca-Sanjuán, D.; Merchán, M.; Serrano-Andrés, L. *Chem. Phys.* **2008**, *349*, 188.

(28) Steenken, S. *Chem. Rev.* **1989**, *89*, 503.

(29) Kumar, A.; Sevilla, M. D. *J. Phys. Chem. B*, in press.

(30) Bertran, J.; Oliva, A.; Rodríguez-Santiago, L.; Sodupe, M. *J. Am. Chem. Soc.* **1998**, *120*, 8159.

(31) Mulliken, R. S. ; Person, W. B. *Molecular Complexes*; Wiley-Interscience: New York, 1969.

(32) Badger, B.; Brocklehurst, B. *Trans. Faraday Soc.* **1969**, *65*, 2576.

(33) Badger, B.; Brocklehurst, B. *Trans. Faraday Soc.* **1969**, *65*, 2582.

(34) Badger, B.; Brocklehurst, B. *Trans. Faraday Soc.* **1969**, *65*, 2588.

(35) Pieniazek, P. A.; Krylov, A. I.; Bradforth, S. E. *J. Chem. Phys.* **2007**, *127*, 044317.

(36) Pieniazek, P. A.; Bradforth, S. E.; Krylov, A. I. *J. Chem. Phys.* **2008**, *129*, 074104.

(37) Pieniazek, P. A.; VandeVondele, J.; Jungwirth, P.; Krylov, A. I.; Bradforth, S. E. *J. Phys. Chem. A* **2008**, *112*, 6159.

(38) Pieniazek, P. A.; Sundstrom, E. J.; Bradforth, S. E.; Krylov, A. I. *J. Phys. Chem. A* **2009**, *113*, 4423.

(39) Müller-Dethlefs, K.; Hobza, P. *Chem. Rev.* **2000**, *100*, 143.

(40) Sponer, J.; Leszczynski, J.; Hobza, P. *Biopolymers* **2002**, *61*, 3.

(41) Saigusa, H. *Photochem. Photobiol.* **2006**, *7*, 197.

(42) de Vries, M. S.; Hobza, P. *Annu. Rev. Phys. Chem.* **2007**, *58*, 585.

(43) Davidson, E. R.; Borden, W. T. *J. Phys. Chem.* **1983**, *87*, 4783.

(44) Russ, N. J.; Crawford, T. D.; Tschumper, G. S. *J. Chem. Phys.* **2004**, *120*, 7298.

(45) Polo, V.; Kraka, E.; Cremer, D. *Mol. Phys.* **2002**, *100*, 1771.

(46) Zhang, Y.; Yang, W. *J. Chem. Phys.* **1998**, *109*, 2604.

(47) Sinha, D.; Mukhopadhyay, D.; Mukherjee, D. *Chem. Phys. Lett.* **1986**, *129*, 369.

(48) Pal, S.; Rittby, M.; Bartlett, R. J.; Sinha, D.; Mukherjee, D. *Chem. Phys. Lett.* **1987**, *137*, 273.

(49) Stanton, J. F.; Gauss, J. *J. Chem. Phys.* **1994**, *101*, 8938.

(50) Nooijen, M.; Bartlett, R. J. *J. Chem. Phys.* **1995**, *102*, 3629.

(51) Golubeva, A. A.; Pieniazek, P. A.; Krylov, A. I. *J. Chem. Phys.* **2009**, *130*, 124113.

(52) Iikura, H.; Tsuneda, T.; Yanai, T.; Hirao, K. *J. Chem. Phys.* **2001**, *115*, 3540.

(53) Baer, R.; Neuhauser, D. *Phys. Rev. Lett.* **2005**, *94*, 043002.

(54) Chai, J.-D.; Head-Gordon, M. *J. Chem. Phys.* **2008**, *128*, 084106.

(55) Chai, J.-D.; Head-Gordon, M. *Phys. Chem. Chem. Phys.* **2008**, *10*, 6615.

(56) Grimme, S. *J. Comput. Chem.* **2004**, *25*, 1463.

(57) Hehre, W. J.; Ditchfield, R.; Pople, J. A. *J. Chem. Phys.* **1972**, *56*, 2257.

(58) Krishnan, R.; Binkley, J. S.; Seeger, R.; Pople, J. A. *J. Chem. Phys.* **1980**, *72*, 650.

(59) Jurečka, P.; Šponer, J.; Černý, J.; Hobza, P. *Phys. Chem. Chem. Phys.* **2006**, *8*, 1985.

(60) Olaso-Gonzáles, G.; Roca-Sanjuán, D.; Serrano-Andrés, L.; Merchán, M. *J. Chem. Phys.* **2006**, *125*, 231002.

(61) Bravaya, K. Private communication.

(62) Pitoňák, M.; Riley, K. E.; Neogrády, P.; Hobza, P. *Comput. Phys. Commun.* **2008**, *9*, 1636.

(63) Sinnokrot, M. O.; Sherrill, C. D. *J. Phys. Chem. A* **2004**, *108*, 10200.

(64) Sinnokrot, M. O.; Sherrill, C. D. *J. Phys. Chem. A* **2006**, *110*, 10656.

(65) Kratochvil, M.; Engkvist, O.; Sponer, J.; Jungwirth, P.; Hobza, P. *J. Phys. Chem. A* **1998**, *102*, 6921.

CT900515A